




TECHNICAL ARTICLE

Effect of Multidirectional Forging on the Microstructure Evolution and Mechanical Properties of Mg-2Sn-2Zn-0.7Mn-0.5Ca Alloys

TAIYU LU,¹ YANDONG YU ^{1,5} ZEHUA YAN,² LIWEI QUAN,^{3,6}
and HAO ZHOU⁴

1.—School of Materials Science and Chemical Engineering, Harbin University of Science and Technology, Harbin 150040, China. 2.—Rongcheng College, Harbin University of Science and Technology, Weihai 264300, China. 3.—School of Materials Science and Engineering, Hebei University of Technology, Tianjin 300401, China. 4.—School of Materials Science and Engineering, Nanjing University of Science and Technology, Nanjing 210094, China. 5.—e-mail: yydhrb@163.com. 6.—e-mail: quanlw@hebut.edu.cn

The Mg-2Sn-2Zn-0.7Mn-0.5Ca (wt.%) alloy was employed to investigate the effect of forging passes on both microstructural and mechanical properties as well as the mechanism of multidirectional forging (MDF). The results show that with the increase of MDF passes, the second phase is fragmented and dispersed. At the same time, the alloy's microstructure exhibits necklace-like microstructures with different thicknesses due to the generation of recrystallized grains. After the alloys are deformed by the first forging pass (MDF-1) and the third forging pass (MDF-3), both the strength and plasticity tend to increase. The strength of MDF-3 passes is the highest (230 MPa), while the elongation is improved in the fifth forging pass (MDF-5) deformed alloy with a concomitant decrease in tensile strength by 11 MPa. This phenomenon occurred because, after the alloy undergoes MDF-5 deformation, the texture changes from a typical basal texture to a bimodal texture. In other words, following MDF treatment, grain refinement and texture weakening together affect the mechanical properties of the alloys.

INTRODUCTION

Magnesium alloys have attracted much attention due to their attractive properties, including low density, favorable castability, elevated specific strength, and commendable recyclability.^{1–4} However, high-temperature deformation of magnesium alloys is still a large challenge. The hexagonal close-packed (HCP) crystal structure of magnesium alloys has limited slip modes that are easily activated, which leads to poor ductility. This constrains their widespread utility in many fields. Improving magnesium alloy mechanical properties is a multifaceted challenge, influenced by many factors such as grain size, texture modulation, heat treatment, and processing. Nowadays, scholars focus on grain refinement and reducing texture intensity to

improve magnesium alloy properties.^{5,6} According to the Hall-Petch relationship, it is proposed that diminishing grain size can improve the yield strength of alloys.^{7,8} Meanwhile, the pronounced anisotropic propensity of texture can significantly influence the properties. Scientists have studied not only the role of texture in deformation mechanics but also the mechanisms governing texture modulation using advanced sophisticated technological methods.^{9–11}

In recent years, researchers have changed the composition of the second phase in magnesium alloy by introducing Sn,¹² Mn,¹³ and rare earth elements^{14,15} into the magnesium matrix, thereby controlling the texture and grain size, leading to improved mechanical properties. Hou et al.¹⁶ explored Mg-Zn-Sn-xMn alloys with different Mn content and discovered that Mn facilitates the nucleation of rod-like MgZn₂ particles, which improves the mechanical properties of the alloy. Yang et al.¹⁷ found that adding a moderate amount

(Received March 21, 2024; accepted June 24, 2024;
published online July 10, 2024)

of Ca to Mg-Zn-Sn alloys promotes the formation of CaMgSn particles. Additionally, adding Zn and Ca to magnesium alloys tends to induce grain boundary segregation, leading to a heterogeneous microstructure with a diminished basal texture. The formation of this structural feature is essential for enhancing the activation of non-basal slip and suppressing the nucleation of twins.

Severe plastic deformation (SPD) is a processing technology capable of significantly refining metal grains,¹⁸⁻²¹ this process including equal channel angular extrusion, cyclic extrusion compression, MDF, accumulated roll bonding, and multi-axial compression. These techniques involve applying very large plastic strains to the material, which alters its microstructure, strengthens the material, and refines its grains. MDF technology has attracted a great deal of attention because of its simplicity and ease of operation.²²⁻²⁴ In a study by Wang et al.,²⁵ MDF processing on Mg-Gd-Y-Zn-Zr-Ag alloys showed that increasing MDF passes led to internal textural changes and grain refinement in the alloy. The MDF processing activated prismatic slip around the transverse directional (TD) axis in deformed grains. Meanwhile, other deformed grains become activated through multiple slip mechanisms, significantly enhancing the mechanical

properties of the alloy. However, the effect of MDF processing on texture and grain characterization is seldom researched in Mg-2Sn-2Zn-0.7Mn-0.5Ca (wt.%) alloy. Therefore, this paper aims to investigate the effects of varying forging passes on the evolution of microstructure, texture, and mechanical properties. The research hopes to elucidate the plastic deformation mechanism of MDF in magnesium alloy and provide a scientific foundation for the practical application of the MDF process.

MATERIALS AND EXPERIMENTAL METHODS

Preparation of Materials

The nominal percentage of material used in this study was Mg-2Sn-2Zn-0.7Mn-0.5Ca (wt.%), which was prepared from high purity Mg, Sn, Zn (~ 99.9 wt.%) and Mg-10 Mn, Mg-30Ca intermediate alloys. After casting, this alloy was subjected to a two-stage solution treatment which was to hold the alloy at 375°C for 2 h and then hold it at 450°C for 6 h. Water-cooling treatment was subsequently followed. Then, the alloy was cut into a billet by wire cutting with dimensions of 14 mm × 14 mm × 20 mm and chamfered R3. Before forging, the specimen was assembled with the MDF molds as shown in

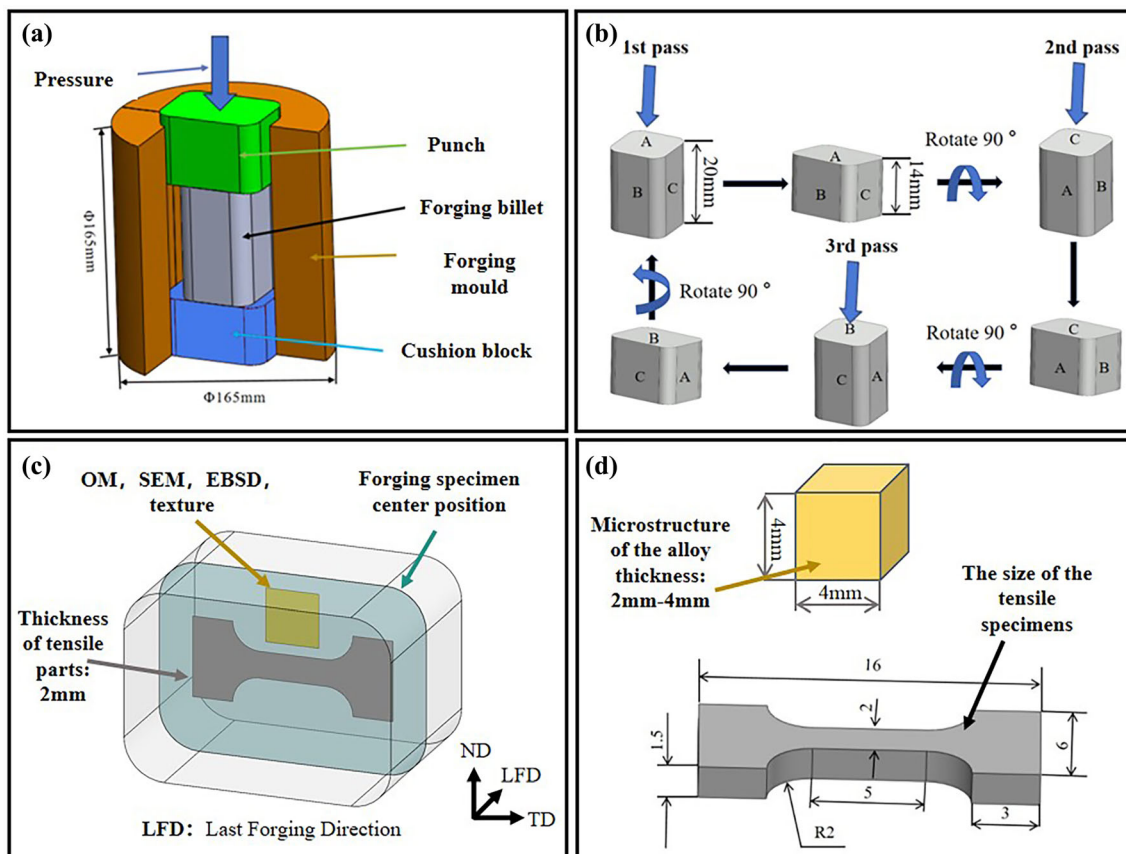


Fig. 1. (a) Schematic diagram of MDF mold, (b) MDF process flow diagram, (c) schematic diagram of sampling location, (d) dimension of specimen for OM and dimension of specimen for tensile test.

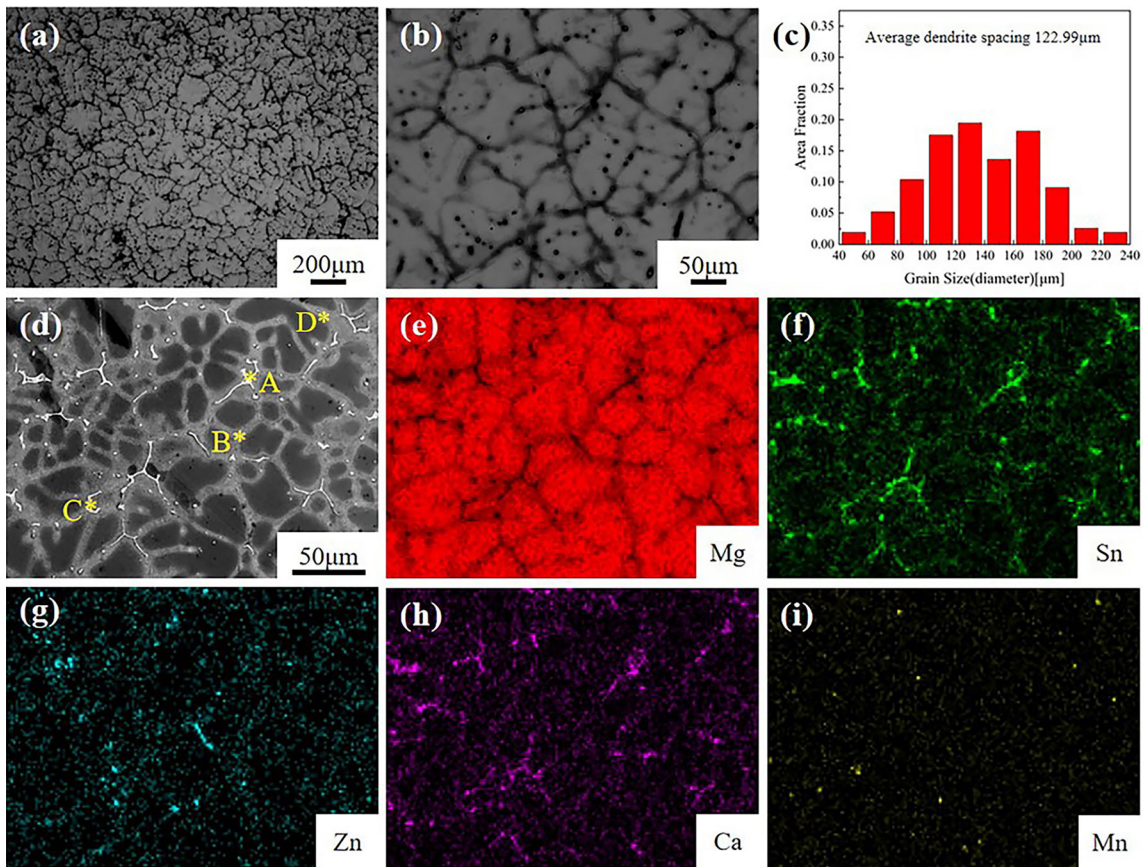


Fig. 2. (a, b) As-cast micrographs, (c) grain size statistics, (d-i) EDS analysis of as-cast Mg - (4-x) Sn-xZn-0.7Mn-0.5Ca alloy.

Fig. 1a. Then, the die and specimen were placed in a resistance furnace together and heated to 325°C holding for 30 min. After heating, the specimen was forged with a downward pressure rate of 20 mm/min and an average strain pass of 0.36 by using a CMT electronic universal testing machine. Next, the specimen was rotated 90° to change another face preparing for the next forging pass as indicated in Fig. 1b.

Microstructure and Mechanical Property Testing

The specimens for optical microscopy (OM), scanning electron microscopy (SEM), electron backscattering diffraction (EBSD), and tensile testing were cut from the center of the MDF specimens as seen in Fig. 1c. The specimens used for OM and SEM were chemically etched with a solution composed of 1.4% picric acid, 6.2% glacial acetic acid, 84% ethanol, and 8.4% distilled water. The microstructural observations were conducted with an Olympus optical microscopy and Inca 350. The EBSD specimens were electropolished using the solution of perchloric acid and acetic acid (AC2). Testing was conducted using a Hitachi SU5000 device, followed by the analysis and processing of the obtained data utilizing AZtecCrystal software. The specimens for the tensile test were dog-bone shaped with a gauge

length of 5 mm, width of 2 mm, and thickness of 1.5 mm depicted in Fig. 1d. Tensile tests were carried out at a strain rate of 0.2 mm/min with the tensile direction parallel to the TD.

RESULTS AND DISCUSSION

Microstructure of the Initial As-Cast and Solid Solution States

Figure 2 shows the micrographs and energy spectra of the as-cast Mg-2Sn-2Zn-0.7Mn-0.5Ca alloy. Figure 2a reveals that the as-cast microstructure of the alloy primarily consists of α -Mg and a second phase, which is reticulate in morphology and predominantly distributed along the grain boundaries. A higher magnification graph in Fig. 2b reveals that the microstructure of the second phase is predominantly lamellar. Additionally, fine granular phases are noticeable adjacent to the eutectic regions. This may be attributed to the slow cooling experienced by this section of the alloy during solidification, leading to the precipitation of second phases within the grains while the alloy cooled to room temperature. The average primary dendrite spacing of the as-cast alloy at this point is approximately 122.99 μm as shown in Fig. 2c. To further investigate the distribution of alloying elements during the casting process, EDS analysis was

conducted as presented in Fig. 2d, e, f, g, h, and i. The figure shows that the elements Zn, Sn, and Ca in the cast Mg-2Sn-2Zn-0.7Mn-0.5Ca (wt.%) alloy are mainly segregated at the grain boundaries and their neighboring regions to form the second phase. The distribution of Mn elements in the alloy is relatively uniform, and this distribution characteristic is conducive to improving the overall performance and weldability of magnesium alloys. Table I presents the EDS analysis results from points A, B, C, and D marked in Fig. 2d. The atomic ratio of Ca to Sn at point A is approximately 1:1, with only a minor presence of Zn, forming elongated stripes. This phase is tentatively identified as the CaMgSn phase. At point B, the Mg to Zn ratio is about 1:2, forming a spherical phase, which is presumed to be the MgZn₂ phase, with the excess Mg being part of the α-Mg matrix. The Mg to Sn ratio is approxi-

mately 2:1 at point C, leading to the deduction that the phase is the Mg₂Sn phase. The component analysis of point D shows that the Mn content is 14.57%. Therefore, it is inferred that this point is an α-Mn phase, with most of it distributed in a granular form in the matrix.

Based on the analysis above, the second phase at the grain boundaries of the cast alloy is relatively coarse. During the subsequent deformation process, cracks are more likely to be generated near the phases at the grain boundaries, thus affecting its plastic-forming ability.²⁶ To improve the supersaturation and plastic-forming ability of the alloy, it is necessary to homogenize the cast alloy. According to related research,²⁷ in Mg-Sn-Zn alloys, a secondary solution treatment is usually required to promote the full diffusion of Sn and Zn in the alloy. The micrographs of the homogenized alloy and its EDS test results are shown in Fig. 3. To allow the Mg-Zn phase to fully dissolve into the alloy matrix and to control the Zn element to diffuse first, the primary solution treatment temperature should be selected between 310°C and 400°C. Figure 3a shows that after the first solution treatment, most of the spherical eutectic phase in the alloy is dissolved into the α-Mg matrix, but a small amount of flaky second phase is still present at the grain boundaries. In addition, after the first solid solution treatment, the average grain size of the alloy slightly increased from 110 μm to 140 μm. After the secondary solution treatment, Fig. 3b shows

Table I. EDS results of Mg - (4-x) Sn-xZn-0.7Mn-0.5Ca alloy as cast (at.%)

Points	Mg	Sn	Zn	Mn	Ca
A	44.08	31.74	0.75	0.31	23.12
B	55.69	1.82	40.21	0.28	0.2
C	63.54	33.94	0.14	0.07	2.31
D	83.92	0.90	0.62	14.57	0.31

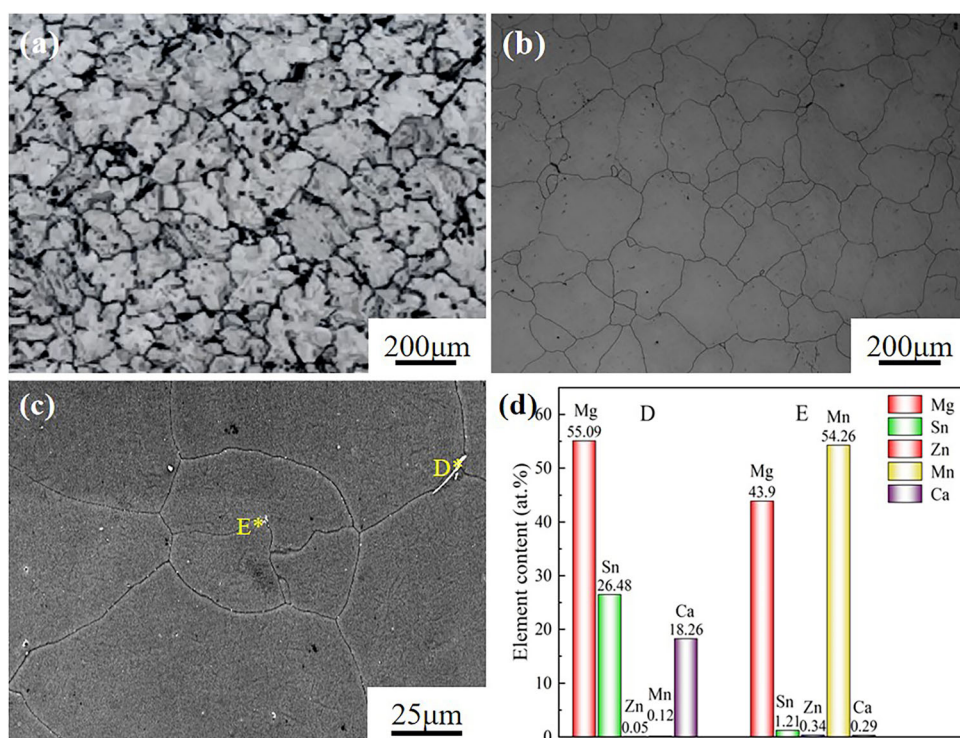


Fig. 3. Micrographs of solid solution alloys and their EDS tests: (a) primary solution treatment, (b) secondary solution treatment, (c) EDS locations, (d) concentration histograms.

that the number of eutectic phases at the grain boundaries of the as-cast alloy was significantly reduced, and only a very small number of elongated phases were present at the grain boundaries. The average grain size of the alloy is about $178\ \mu\text{m}$, $43\ \mu\text{m}$ larger than that of the as-cast alloys. The morphology and composition of cast and homogenized alloys were studied in depth using the EDS test. Point D in the alloy after secondary solution treatment has a Ca/Sn ratio of about 1:1, which is presumed to be the CaMgSn phase. While the content of Mn in position E is as high as 54.26%, it can be presumed to be the monolithic Mn, as shown in Fig. 3c and d.

Influence of the Forging Passes on the Microstructure of the Alloy

To investigate the influence of the forging passes on the microstructures of Mg-2Sn-2Zn-0.7Mn-0.5Ca alloy, the microstructure was observed in the alloys of MDF-1, MDF-3, and MDF-5 forged alloys, and the results are shown in Fig. 4. After the MDF-1 deformation, the microstructure of the alloy is characterized by many coarse deformed grains and fine recrystallized grains around their grain boundaries, and the direction of elongation of the coarse grains is perpendicular to the forging direction of the specimen. Compared with the solid solution state, the coarse grains in the MDF-1 alloy were elongated, and fewer recrystallized grains appeared

at the grain boundaries, as shown in Fig. 4a. When the alloy is deformed by MDF-3, the grain size within the alloy is significantly reduced compared with that of MDF-1 alloy, while the number of recrystallized grains is significantly increased. At the same time, these recrystallized grains are surrounded by the grain boundaries of the coarse grains, and the “necklace” structure is more obvious, as shown in Fig. 4d. When the alloy is deformed by MDF-5, the degree of recrystallization of the alloy is further enhanced, and the grains are more homogeneous compared with MDF-3, as shown in Fig. 4g. Figure 4b, e, and h illustrates the scanning electron microscope images of the secondary phase in the alloy under different forging passes. As marked by the yellow box in Fig. 4b, many fine dynamic precipitation phases are observed in the MDF-1 alloy. This is due to the dynamic precipitation of the second phase during the holding and forging stages. When the forging passes are increased to MDF-3, the distribution of the second phase becomes more irregular and is located mainly at the boundaries of the dynamically recrystallized grains. The reason is that the local strain field during the forging process promotes the nucleation and growth of recrystallization by enhancing the diffusion of solute atoms, as shown by the yellow box in Fig. 4e.²⁸ With further increase of the forging passes up to MDF-5, the local strain field during forging increases, the grain size of the alloy refines, and the second phase becomes more dispersed as

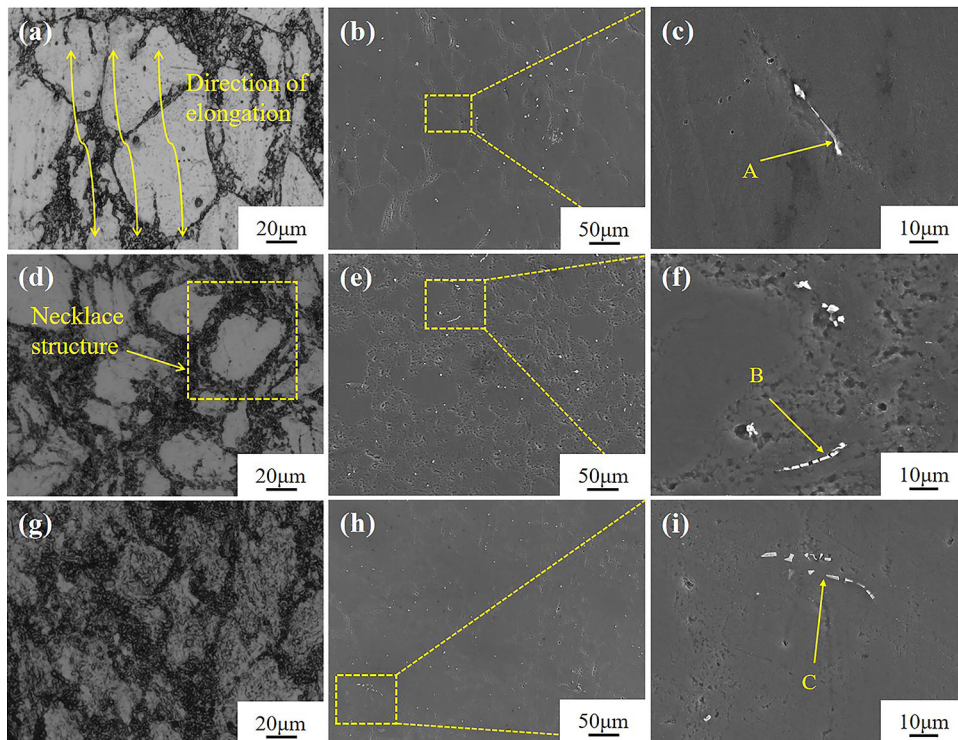


Fig. 4. Metallographic and SEM images of Mg-2Sn-2Zn-0.7Mn-0.5Ca alloy after different passes of MDF: (a, b, c) MDF-1, (d, e, f) MDF-3, (g, h, i) MDF-5.

Table II. EDS results of Mg-2Sn-2Zn-0.7Mn-0.5Ca alloys with different MDF passes (at.%)

Points	Mg	Sn	Zn	Mn	Ca
A	55.64	23.42	0.60	0.17	20.17
B	54.59	0.97	2.56	40.94	0.74
C	74.60	12.35	1.96	0.42	10.67
D	79.92	9.79	1.31	0.34	8.64

shown in Fig. 4g, h, and i. Figure 4c, f, and i presents the enlarged images within the yellow dashed boxes in Fig. 4b, e, and h. EDS examination of the long stripes of the second phase is shown in Table II. The ratio of Ca and Sn atomic contents at points A, C, and D in Fig. 4c, f, and i is close to 1:1, which is close to 1:1. Meanwhile, according to the B-peak plot in Fig. 2c, it is known that the CaMgSn phase exists in the alloy. This shows that the elongated second-phase particles should be CaMgSn phase. When the deformation was carried out to MDF-3 passes, the elongated CaMgSn phase in the alloy was fragmented and refined, and the distribution of the CaMgSn phase in the alloy was more uniform after MDF-5 passes. Analyzing the point B marked in Fig. 4f showed that this point is the area of manganese aggregation, and the atomic percentage content of manganese is about 40.94%. Therefore, the second phase corresponding to point B is α -Mn particles. In conclusion, when the number of forging passes of the alloy was increased from 1 to 5 passes, the grain refinement of the alloy was significantly increased, which indicates that grain refinement can be effectively achieved by adjusting the number of MDF passes.

Mechanical Properties of the MDFed Alloy

The stress-strain curves of Mg-2Sn-2Zn-0.7Mn-0.5Ca alloy before forging and after deformation in different passes are shown in Fig. 5. From Fig. 5, it is easy to see that the ultimate tensile strength (UTS), tensile yield strength (TYS), and EL of the solid solution state alloy are 176 MPa, 96 MPa, and 12.7%, respectively. The mechanical properties of the alloy have been improved to different degrees after MDF. The UTS, TYS, and EL of the alloy after MDF-1 pass deformation were 195 MPa, 143 MPa, and 15.4%, respectively, which were improved by 19 MPa, 47 MPa, and 2.7% compared to the solid solution state. This was attributed to the finer grain size of the alloy in the deformed state compared to the solid solution state alloy, as well as the change in the size and distribution of the Ca-containing eutectic phases, which improved its strength and plasticity. After the alloy was deformed by MDF-3 the UTS, TYS, and EL of the alloy reached 230 MPa, 193 MPa, and 17.3%, respectively, whereas after the alloy was deformed by MDF-5 its UTS, TYS, and EL were 219 MPa, 167 MPa, and

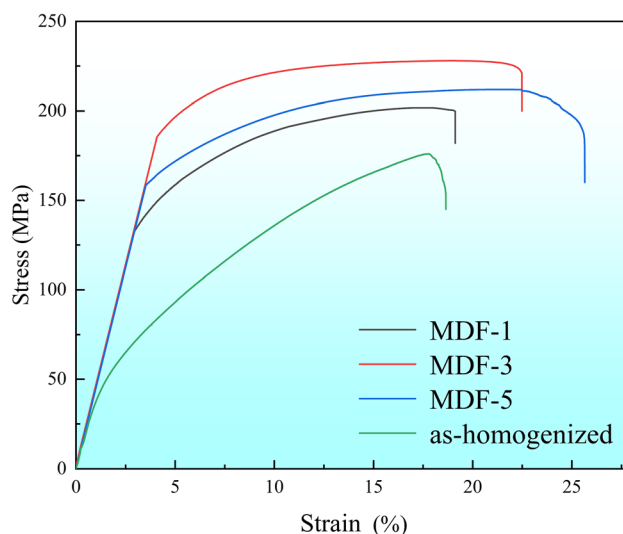


Fig. 5. Tensile stress-strain curves of Mg-2Sn-2Zn-0.7Mn-0.5Ca alloy in solid solution and forged states.

20.3%, respectively. It can be clearly found that the TYS, UTS, and EL of the alloy increased with the increase of the forging passes. Meanwhile, the “necklace-like” microstructure in the alloy resulted in the highest TYS of the MDF-3 pass specimen, and at the same time the specimens showed a good strength-plasticity balance. However, when the specimens were carried out to MDF-5 passes, the degree of DRX reached the highest and the TYS and UTS of the specimens show a decreasing trend, but the EL is the highest. The high strength of the MDF-3 channeled specimens suggests that the coarse deformed grains play an important role in storing dislocations, thus enhancing the UTS of the alloy.

Grain Orientation and Size

Figure 6 shows the IPF maps of Mg-2Sn-2Zn-0.7Mn-0.5Ca alloys with various MDF-1, MDF-3, and MDF-5 forging passes. The grain color maps located in the lower left corner of Fig. 6a, c, and e illustrate the orientation of the grains, where red represents grains inclined towards the (0001) basal plane, while blue and green denote a preference for the (01-10) and (-12-10) prismatic planes, respectively. An analysis of the IPF maps in Fig. 6a and c reveals that red and purple grains are predominant in the MDF-1 and MDF-3 specimens, suggesting that a substantial portion of the grains are aligned with the (0001) plane parallel to the ND basal plane texture. It can be seen that the quantity of blue and green color grains increases clearly from the IPF maps in Fig. 6e. This indicates a transition toward a more randomly oriented grain structure, which can be attributed to the increased number of forging passes that promote a more homogeneous deformation and dynamic recrystallization process. Figure 6b, d, and f shows the grain size distribution

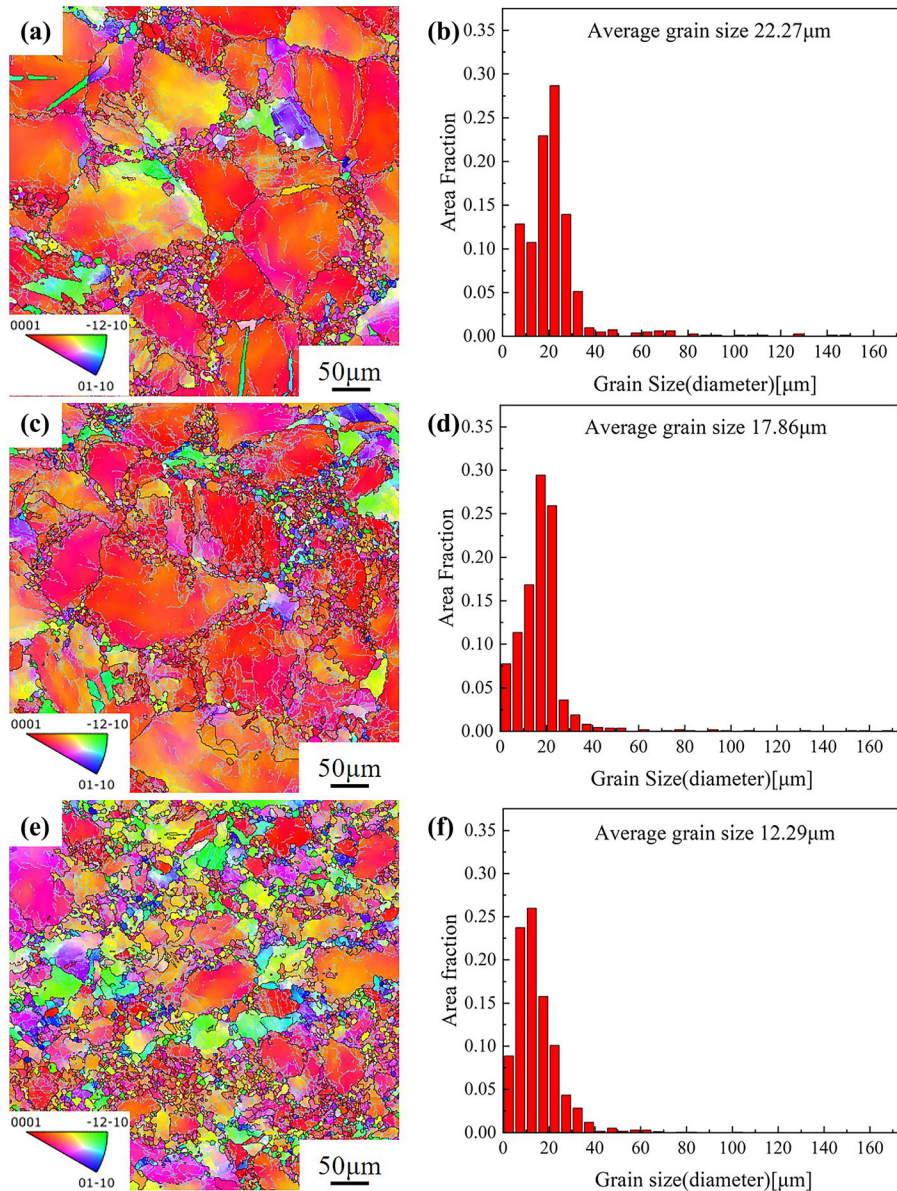


Fig. 6. IPF plots and grain size of Mg-2Sn-2Zn-0.7Mn-0.5Ca alloys with different passes: (a, b) MDF-1, (c, d) MDF-3, (e, f) MDF-5.

of the specimens. These figures demonstrate a clear trend that the quantity of coarse grains significantly diminishes, while the quantity of fine grains increases with an increasing of the MDF passes. This grain refinement is a consequence of repeated plastic deformation and dynamic recrystallization during the MDF process, which leads to a refined microstructure that produces the effect of fine grain reinforcement, improving the strength of the alloy. After MDF-1 passes, the grain size of the alloy decreases from $178 \mu\text{m}$ in the solid solution state to $22.27 \mu\text{m}$. At this time, the alloy grain size varies considerably, with a coarse grain size of up to $170 \pm 0.5 \mu\text{m}$, and the proportion of grain sizes $> 40 \mu\text{m}$ is 4.76%, as shown in Fig. 6b. After MDF-3 and MDF-5 passes, the average grain sizes of the alloys are $17.86 \mu\text{m}$ and $12.29 \mu\text{m}$, respectively, and

the coarse grain sizes are $167 \pm 0.5 \mu\text{m}$ and $102 \pm 0.5 \mu\text{m}$, respectively, as shown in Fig. 6d and e. The percentages of the grains $< 40 \mu\text{m}$ were 3.24% and 2.46%, respectively. An increase of MDF passes not only leads to the fragmentation of coarse grains, which reduces their maximum grain sizes, but also promotes the generation of dynamic recrystallization (DRX) grains, which increases the quantity of the small grains. The DRX process contributes to the weakening of the texture and further grain refinement. The underlying cause of this phenomenon is that many grains need to be reoriented to respond to the applied stress, which subsequently leads to a reduction of the original texture during DRX, which subsequently leads to the mitigation of the original texture, as supported by literature references.^{29,30}

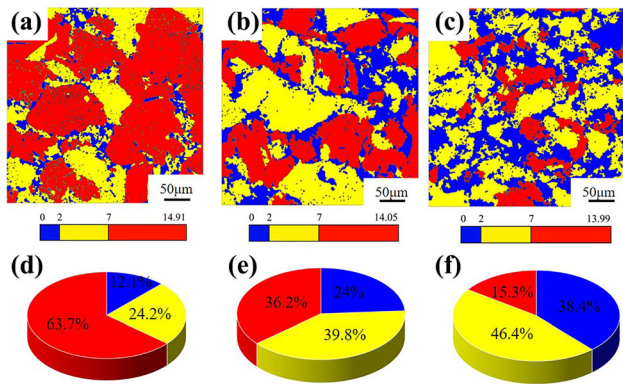


Fig. 7. Recrystallization and ratio of Mg-2Sn-2Zn-0.7Mn-0.5Ca alloys with different passes of MDF: (a) GOS map of MDF-1 lane, (b) GOS map of MDF-3 lanes, (c) GOS map of MDF-5 lanes, (d)-(f) recrystallization volume fractions.

Recrystallization Mechanism

To elucidate the impact of forging passes on the degree of recrystallization in the Mg-2Sn-2Zn-0.7Mn-0.5Ca alloy, the recrystallization was analyzed by using grain orientation spread (GOS) plots on the specimens with different forging passes as presented in Fig. 7. The red, yellow, and blue colors in the figure represent deformed grains, substructured grains, and recrystallized grains of the alloy with different forging passes, respectively. Comparison with Fig. 7a, b, and c shows that the DRXed grains in the three states of alloys are concentrated around the coarse grains, forming a “necklace” structure, and become more uniform as the number of forging passes increases. Furthermore, Fig. 7d, e, and f illustrates that increasing the number of MDF forging passes not only promotes the gradual deformation and crushing of coarse grains but also increases the number of DRXed grains. The volume fraction of DRXed grains in the MDF-1 alloy is about 12.1% compared to 24% in the MDF-3 alloy, and it rises to 38.4% in the MDF-5 alloy. Typically, when the number of MDF passes is below six, coarse grains within the alloy are mechanically divided and refined, and a few fractions of DRXed grains are generated in the deformation zones, which is consistent with the authors such as Zhang et al.^{31,32}

Texture Evolution During the MDF Process

Figure 8 shows pole figure maps of the Mg-2Sn-2Zn-0.7Mn-0.5Ca alloy after deformation by MDF-1, MDF-3, and MDF-5 passes. When the alloy is deformed by MDF-1 passes, the grains are aligned along the (0001) base plane, which is parallel to the longitudinal direction (LD), as shown in Fig. 8a. This alignment occurs because the basal texture is facilitated after deformation. Meanwhile, as shown in Fig. 8b, the (0001) basal plane texture of the deformed alloy of MDF-3 is approximately a 40° deviation from the TD towards the LD. Before MDF-3 forming, the alloy underwent two 90° rotational

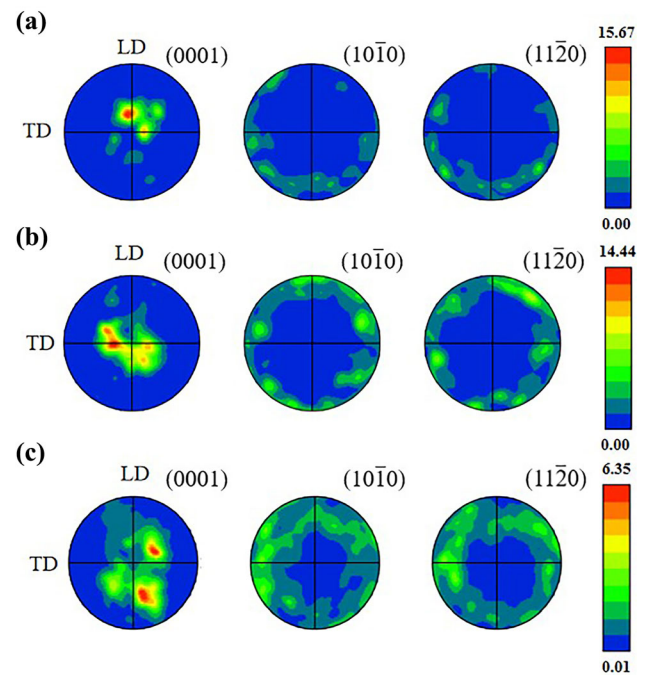


Fig. 8. Polar figure maps of Mg-2Sn-2Zn-0.7Mn-0.5Ca alloys in EBSD: (a) MDF-1, (b) MDF-3, (c) MDF-5.

forging passes, causing a basal plane deflection during MDF-3 deformation. After the MDF-5 deformation, a pronounced bimodal texture emerged. The texture was distributed along the LD direction on the (0001) basal plane. In terms of texture distribution, it is more dispersed than those of MDF-1 and MDF-3, as illustrated in Fig. 8c. The texture of the alloy becomes more dispersed and exhibits a larger deviation angle after MDF-5 deformation. The primary reason for this phenomenon is that multiple forging passes induce expansion and textural deflection at the (0001) basal plane, which activates non-basal slip systems, leading to grain refinement and reduced anisotropy in the alloy.^{33,34} These findings are consistent with other authors such as Che et al.³⁵

ANALYSIS AND DISCUSSION

Microstructure Evolution

To better understand the impact of MDF on grain changes, Fig. 9 shows a schematic diagram of the microstructure adjustment mechanism of Mg-2Sn-2Zn-0.7Mn-0.5Ca alloy. Upon solid solution treatment, Fig. 9a and b indicates a reduction in the second phase of the alloy, accompanied by grain growth. When the alloy was initially forged, many deformed grains appeared in the alloy, these coarse deformed grains elongated significantly under the external force, and their tensile direction became perpendicular to the compression direction of the specimen. At the same time, more recrystallized grains appear at the second phase particles, and these recrystallized grains form a “necklace-like”

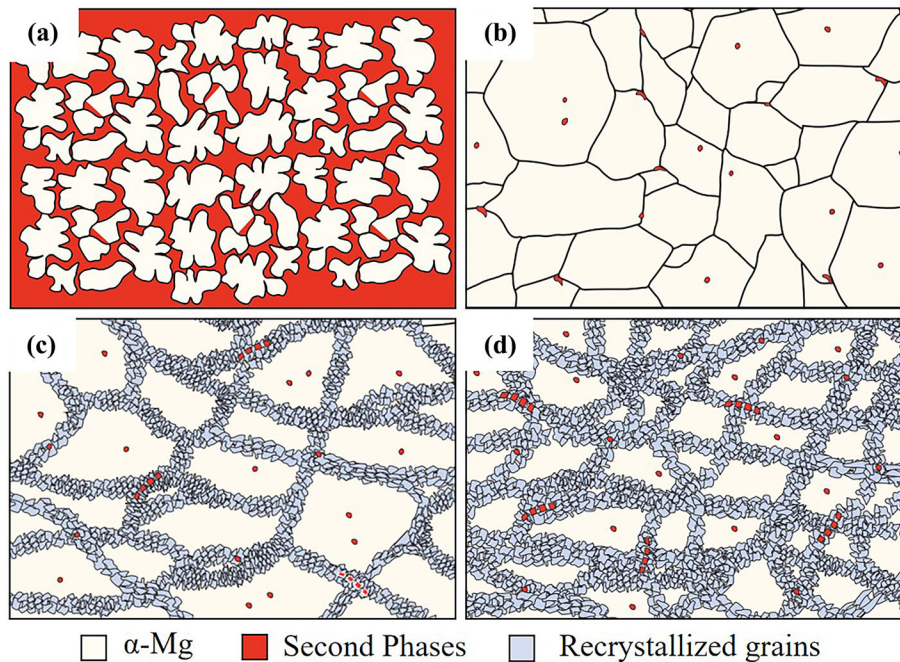


Fig. 9. Schematic diagram of microstructure regulation mechanism of Mg-2Sn-2Zn-0.7Mn-0.5Ca alloy: (a) cast state, (b) solution treatment, (c) primary forging, (d) after multiple forging passes.

microstructure around the deformed grains, as shown in Fig. 9c. As the number of forging passes increases, both the deformed grains and the second-phase particles in the alloy broke up. This resulted in second-phase particles becoming the nucleation point of the recrystallized grains, increasing the degree of recrystallization of the alloy. A more pronounced “necklace-like” microstructure formed around the broken deformed grains, as shown in Fig. 9d.

Effect of Second Relative Mechanical Properties

To investigate the distribution of the second phase within the alloys and its influence on recrystallization nucleation, the second phase in the alloys subjected to varying numbers of forging passes was characterized. Figure 10 illustrates the distribution of the second phase in the Mg-2Sn-2Zn-0.7Mn-0.5Ca alloy after undergoing MDF-1, MDF-3, and MDF-5 deformations. Figure 10a, b, and c indicates that there are fewer recrystallized grains surrounded by coarser Mn particles after MDF-1 deformation. This phenomenon is attributed to the rapid movement rate of grain boundaries due to strain-induced recrystallization nucleation at lower strains. Under these conditions, the effect of second-phase particle-induced recrystallization nucleation is overshadowed by the dominant strain-induced nucleation mechanism.³⁶ Following MDF-3 deformation, the internal Mn and CaMgSn particles within the alloy are refined and become more uniform as they fragment under the influence of forging stresses. The fine dispersion of Mn particles enhanced their

effectiveness in hindering the growth of recrystallized grains during the deformation process of the alloy, thereby reducing the grain size and resulting in a relative increase in the number of grain boundaries. This increase in grain boundaries helped to impede crack propagation, thereby enhancing the strength and toughness of the alloy. The spacing becomes smaller and the second phase particles impede dislocation motion, leading to a significant increase in the volume fraction of recrystallized grains at this time, as demonstrated in Fig. 10d, e, and f. This suggests that the refinement and homogenization of the second phase may facilitate the nucleation of recrystallized grains, contributing to the overall recrystallization process. As depicted in Fig. 10e, the blue-colored regions represent areas of low dislocation density, which is attributed to the consumption of dislocations by the nucleation of recrystallized grains. At this stage, recrystallization within the alloy is primarily initiated by a combination of second-phase particles and strain-induced nucleation. This dual initiation occurs because recrystallized grains originating from second-phase particles exhibit comparable interfacial mobility to those formed by other nucleation mechanisms. Additionally, the high dislocation density surrounding the second-phase particles is rapidly depleted, fostering the nucleation of recrystallization.³⁷ Upon subjecting the alloy to MDF-5 deformation, more finely dispersed phases are generated within the alloy. These phases are predominantly distributed along the grain boundaries of the recrystallized grains, as evidenced in Fig. 10g, h, and i. Under this forging condition, the

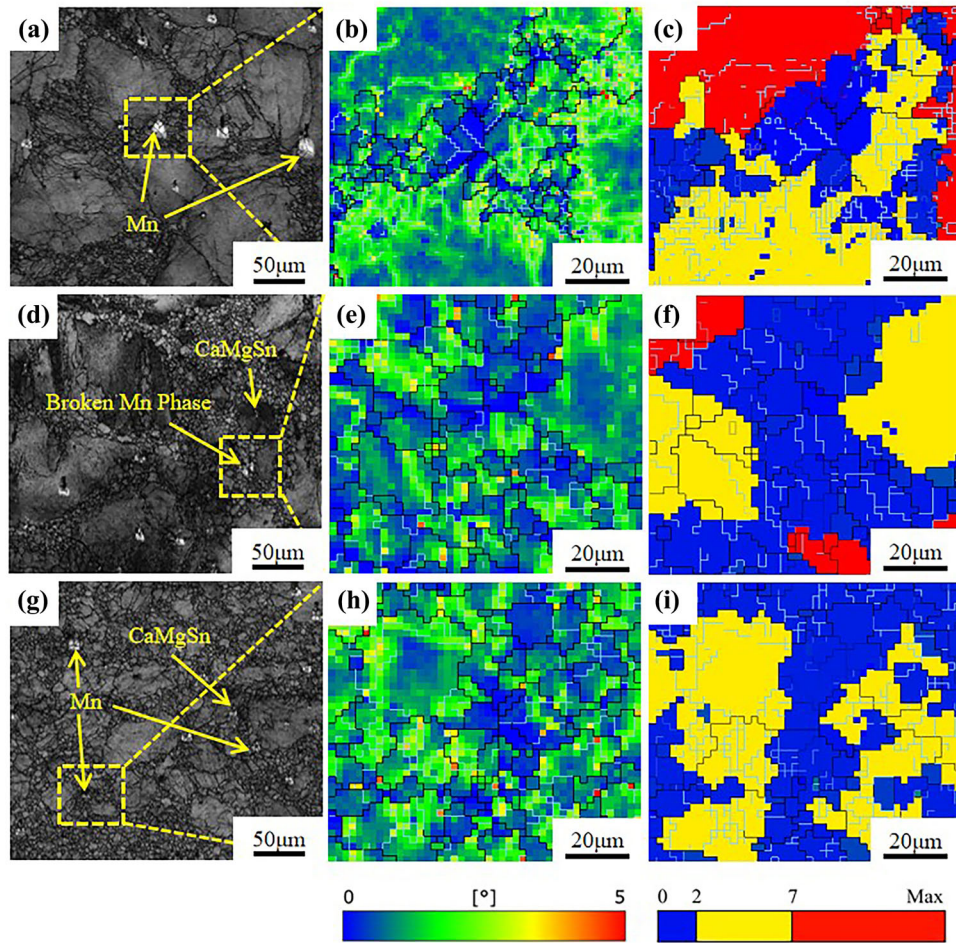


Fig. 10. Second-phase distribution of MDF for Mg-2Sn-2Zn-0.7Mn-0.5Ca alloys with 1, 3, and 5 passes: (a, d, g) EBSD band contrast map, (b, e, h) localized KAM plots, (c, f, i) localized GOS maps.

second-phase particles within the alloy serve as nucleation sites for recrystallized grains, thereby accelerating the recrystallization process. Improve the degree of recrystallization of the alloy and effectively inhibit the growth of the grains, thus promoting further refinement of the alloy grains.

Effect of Dislocations on Mechanical Properties of Alloys

The kernel average misorientation (KAM) represents the average value of the misorientation angle at the grain boundary. When the density of dislocations increases, more interactions among dislocations occur. The interactions among dislocations make it difficult for the lattice in the alloy to slip and deform.³⁸ Therefore, a higher KAM value in an alloy indicates a higher dislocation density and a higher degree of plastic deformation.^{39–41} To investigate the plastic evolution mechanism of the alloy, it is crucial to characterize the KAM values of the Mg-2Sn-2Zn-0.7Mn-0.5Ca alloy after various passes of MDF deformation. The results of these measurements are presented in Fig. 11. Figure 11a, c, and e shows the KAM maps of the region of Fig. 6a, c, and

e. There are many green areas at the coarse grains and their grain boundaries, while the interior of the DRXed grains is blue. This phenomenon showed that due to the continuous accumulation of strain, dislocations accumulate in the coarse grains, resulting in a larger dislocation density in the coarse grain and a smaller dislocation density in the DRXed grains during the MDF process. The results show that the proportion of high KAM values in the alloy decreases progressively following MDF-1, MDF-3, and MDF-5 deformations. The corresponding average KAM values were subsequently determined to be 1.029°, 1.089°, and 0.776°, respectively, as illustrated in Fig. 11b, d, and f. This trend is attributed to the fact that an increased number of forging passes induces greater strain in the alloy, which promotes the formation of numerous new grains by encouraging more grains to achieve the conditions necessary for DRX, leading to a decrease in KAM values within this region.¹⁴ KAM values suggest that after MDF-5 deformation, the formation of recrystallized grains within the alloy consumes lots of dislocations, reduces its KAM value, and facilitates the activation of grain slip, thereby

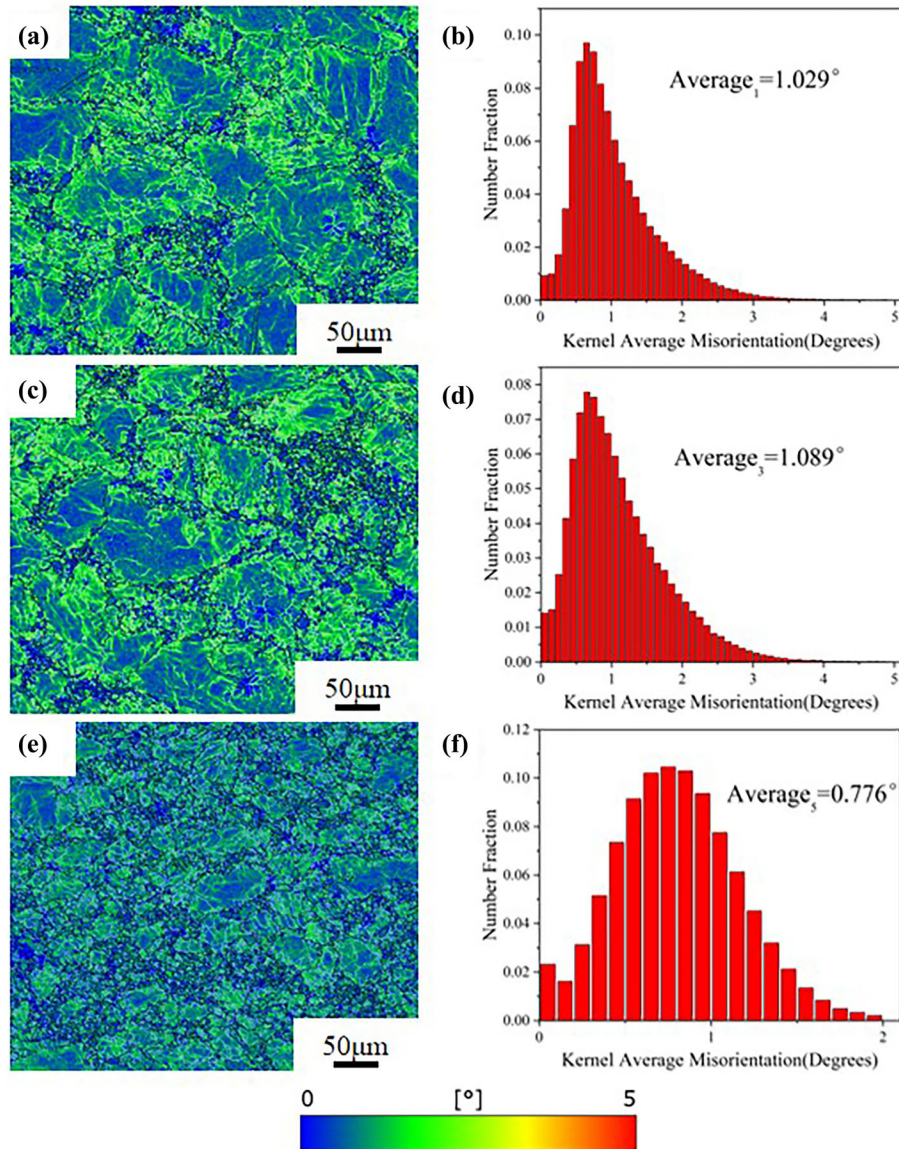


Fig. 11. KAM maps of Mg-2Sn-2Zn-0.7Mn-0.5Ca alloys treated with MDF: (a, b) MDF-1, (c, d) MDF-3, (e, f) MDF-5.

enhancing the alloy's plasticity and increasing its elongation (EL).

From the pole figure maps of the Mg-2Sn-2Zn-0.7Mn-0.5Ca alloy, it is evident that the volume fraction of recrystallization progressively augments with an increase in the number of MDF passes, concomitant with a gradual reduction in texture strength. After MDF-3 pass deformation, the DRX volume fraction of the Mg-2Sn-2Zn-0.7Mn-0.5Ca alloy increased by 11.9% compared to the MDF-1 deformation. However, its texture strength decreased by only 1.23. At this point, the strengthening effect of grain refinement was dominant, leading to an increase in both the strength and elongation of the alloy. When the alloy was subjected to MDF-5 deformation, its DRX volume fraction rose to 38.4%, while the texture strength fell to 6.35, and the texture shifted from the typical

basal type to a bimodal distribution. At that time, the strengthening effect due to grain refinement was surpassed by the softening effect resulting from the weakened texture, allowing for an improvement in the alloy's EL after MDF-5 deformation, albeit at the cost of some strength.

CONCLUSION

The effect of the MDF process on the microstructure, recrystallized grains, texture, and mechanical properties of the Mg-2Sn-2Zn-0.7Mn-0.5Ca (wt.%) alloy was investigated after various forging passes. The conclusions are as follows:

1. The as-cast microstructure of the Mg-2Sn-2Zn-0.7Mn-0.5Ca alloy is composed of α -Mg, Mg_2Sn , $MgZn_2$, and $CaMgZn$ phases. After solution treatment, the majority of the second phase

particles dissolve into the matrix, remaining only a minor quantity of elongated CaMgZn and spherical Mn particles.

- During the MDF deformation, second-phase particles such as the CaMgZn are broken, serving as nucleation sites to facilitate the nucleation of recrystallization and promote the recrystallization of the alloy. The coarse grains underwent significant elongation and fragmentation, forming a “necklace” structure characterized by fine grains surrounding larger deformed grains. The average grain sizes of the MDF-1, MDF-3, and MDF-5 alloys are 22.27 μm , 17.86 μm , and 12.29 μm , respectively.
- After the alloys are deformed by MDF-1 and MDF-3 passes, both the strength and toughness tended to increase when the alloy was forged in MDF-5; the texture of the (0001) basal plane shifted and activated the non-basal plane slip system with a pronounced bimodal texture. This causes the weakening effect of the alloy texture to be greater than the strengthening effect of grain refinement, resulting in an increase in the EL of the alloy but a decrease in tensile strength of 20 MPa.

AUTHOR CONTRIBUTIONS

Taiyu Lu: Conceptualization, Methodology, Data curation, Visualization, Investigation, Writing—original draft preparation. Yandong Yu: Supervision, Data curation, Project administration, Writing—review and editing, Funding acquisition. Zehua Yan: Data curation, Visualization, Writing—review and editing. Liwei Quan: Writing—review and editing. Hao Zhou: Writing—review & editing.

FUNDING

This work was supported by the Talent Training Project of the Central Government's Reform and Development Funds for Local Universities (Grant Number [2021] 137).

DATA AVAILABILITY

Data will be made available on request.

CONFLICT OF INTEREST

All authors certify that they have no affiliations with or involvement in any organization or entity with any financial interest or non-financial interest in the subject matter or materials discussed in this manuscript.

REFERENCES

- X. He, J.D. Liu, C. Yang, and G. Jiang, *Comput. Mater. Sci.* 223, 112111 <https://doi.org/10.1016/j.commatsci.2023.112111> (2023).
- D.L. Yin, K.F. Zhang, G.F. Wang, and W.B. Han, *Mater. Sci. Eng. A* 392, 320 <https://doi.org/10.1016/j.msea.2004.09.039> (2005).
- S. Jayasathyakawin, M. Ravichandran, N. Baskar, C.A. Chairman, and R. Balasundaram, *Today Proc.* 27, 909 <https://doi.org/10.1016/j.matpr.2020.01.255> (2020).
- V.P. Astakhov, Mechanical and industrial engineering: historical aspects and future directions, in *Mechanical and industrial engineering: historical aspects and future directions*. ed. by J.P. Davim (Springer, New York, 2022), pp. 39–93.
- K. Abhishek, R.K. Rahul, and O. Rajkumar, *Mater. Today Proc.* <https://doi.org/10.1016/j.matpr.2023.03.448> (2023).
- B.D. Shi, C. Yang, Y. Peng, F.C. Zhang, and F.S. Pan, *J. Magnes. Alloys* 10, 1476 <https://doi.org/10.1016/j.jma.2022.03.006> (2022).
- M.R. Castelino, Mallikappa, and S.K. Karinka, *Mater. Today Proc.* <https://doi.org/10.1016/j.matpr.2023.05.178> (2023).
- M.R. Barnett, *Mater. Sci. Eng. A* 464, 1 <https://doi.org/10.1016/j.msea.2006.12.037> (2007).
- S. Liu, Ch. Wang, H. Ning, Z.Y. Meng, K. Guan, and H.Y. Wang, *J. Magnes. Alloys* 1, 7 <https://doi.org/10.1016/j.jma.2023.01.017> (2023).
- D. Liu, Z.Y. Liu, and E. Wang, *Mater. Sci. Eng. A* 612, 208 <https://doi.org/10.1016/j.msea.2014.06.034> (2014).
- H.Y. Wang, J. Rong, Z.Y. Yu, M. Zha, Ch. Wang, Z.Z. Yang, R.Y. Bu, and Q.C. Jiang, *Mater. Sci. Eng. A* 697, 149 <https://doi.org/10.1016/j.msea.2017.05.000> (2017).
- P. Vignesh, G. Venkatesh, and S. Kumaran, *Mater. Today Proc.* 27, 2445 <https://doi.org/10.1016/j.matpr.2019.09.215> (2020).
- H.S. Xue, S. Liu, W. Xie, Y. Zhou, J.B. Peng, H.T. Pan, D.F. Zhang, and F.S. Pan, *Mater. Charact.* 187, 111874 <https://doi.org/10.1016/j.matchar.2022.111874> (2022).
- H.T. Jeong, and W.J. Kim, *J. Magnes. Alloys* 10, 2901 <https://doi.org/10.1016/j.jma.2022.01.006> (2022).
- W.J. Ci, L.L. Deng, X.H. Chen, X. Dai, L. Feng, C. Wen, J.Y. Bai, and F.S. Pan, *J. Mater. Res. Technol.* 26, 4107 <https://doi.org/10.1016/j.jmrt.2023.08.166> (2023).
- C.H. Hou, F.G. Qi, Z.S. Ye, N. Zhao, D.F. Zhang, and X.P. Ouyang, *Mater. Sci. Eng. A* 774, 138933 <https://doi.org/10.1016/j.msea.2020.138933> (2020).
- M.B. Yang, L. Cheng, and F.S. Pan, *Trans. Nonferrous Met. Soc. China* 20, 769 [https://doi.org/10.1016/S1003-6326\(09\)60212-0](https://doi.org/10.1016/S1003-6326(09)60212-0) (2010).
- X.D. Sun, X.J. Hao, J.F. Nie, Y. Fan, Y.Y. Chen, S.D. Liu, X.F. Liu, and Y.H. Zhao, *J. Mater. Res. Technol.* 21, 532 <https://doi.org/10.1016/j.jmrt.2022.09.037> (2022).
- P.C. Sharath, Multidirectional forging, in *Multidirectional forging: an advanced deforming technique for severe plastic deformation*. ed. by J. Paulo-Davim, and K. Gupta (Elsevier, New York, 2021), pp. 529–556. <https://doi.org/10.1016/B978-0-12-822049-8.00017-7>.
- M. Kasaeian-Naeini, M. Sedighi, and R. Hashemi, *J. Magnes. Alloys* 10, 938 <https://doi.org/10.1016/j.jma.2021.11.006> (2022).
- A. Heczal, F. Akbaripanah, M.A. Salevati, R. Mahmudi, Á. Vida, and J. Gubicza, *J. Alloys Compd.* 763, 629 <https://doi.org/10.1016/j.jallcom.2018.06.002> (2018).
- J.H. Zhao, Y.L. Deng, and J.G. Tang, *J. Mater. Res. Technol.* 9, 8001 <https://doi.org/10.1016/j.jmrt.2020.05.033> (2020).
- B.B. Dong, X. Che, Z.M. Zhang, J.M. Yu, and M. Meng, *J. Alloys Compd.* 881, 160561 <https://doi.org/10.1016/j.jallcom.2021.160561> (2021).
- A. Jamali, and R. Mahmudi, *Mater. Sci. Eng. A* 752, 426 (2019).
- J.K. Wang, C.M. Liu, S.N. Jiang, and G. Zeng, *J. Mater. Res. Technol.* 24, 3548 <https://doi.org/10.1016/j.jmrt.2023.04.076> (2023).
- J.J. Lewandowski, and M. Seifi, *Annu. Rev. Mater. Res.* 46, 151–186 <https://doi.org/10.1146/annurev-matsci-070115-032024> (2016).
- J. Wang, J.J. Han, B.N. Du, Y.X. Huang, L.Y. Sheng, W.F. Rao, C.P. Wang, and X.J. Liu, *Calphad* 58, 6 <https://doi.org/10.1016/j.calphad.2017.03.008> (2017).

28. L.L. Huang, C.X. Wang, X.K. Liu, P. Liu, X.H. Chen, P.X. Mei, L. Wei, F.C. Ma, and D.H. He, *Nonferrous Metal. Mater. Eng.* 38(4), 215–221 (2017).
29. M.T. Andani, A. Lakshmanan, V. Sundararaghavan, J. Alison, and A. Misra, *Acta Mater.* 226, 117613 <https://doi.org/10.1016/j.actamat.2021.117613> (2022).
30. G.Q. Wu, J.M. Yu, L.C. Jia, W.L. Xu, B.B. Dong, Z.M. Zhang, and B.Y. Hao, *Mater.* 13, 32 <https://doi.org/10.3390/MA13214932> (2020).
31. J.L. Zhang, H. Xie, Z.L. Lu, Y. Ma, S.P. Tao, and K. Zhao, *Results Phys.* 10, 967 <https://doi.org/10.1016/j.rinp.2018.08.028> (2018).
32. N. Bian, F. Li, H.Q. Du, W.T. Niu, and Z.Y. Chen, *J. Alloys Compd.* 923, 166248 <https://doi.org/10.1016/j.jallcom.2022.166248> (2022).
33. B. Liu, J. Yang, X.Y. Zhang, Q. Yang, J.S. Zhang, and X.Q. Li, *J. Magnes. Alloys* 11, 15 <https://doi.org/10.1016/j.jma.2022.12.015> (2023).
34. M.O. Markushev, *Phys. Met. Metallogr.* 108, 43 <https://doi.org/10.1134/S0031918X09070060> (2009).
35. X. Che, B. Dong, Q. Wang, K. Liu, and Z. Zhang, *J. Alloys Compd.* 854, 156264 <https://doi.org/10.1016/j.jallcom.2020.156264> (2021).
36. Z.Q. Li, and J.S. Wang, *Aerospace Manufact. Technol.* 64, 93 <https://doi.org/10.16080/j.issn1671-833x.2021.09.093> (2021).
37. F.J. Humphreys, *Acta Metall.* 25, 1323 (1977).
38. B.Q. Shi, Y.Q. Cheng, X.L. Shang, H. Yan, R.S. Chen, and W. Ke, *Mater. Sci. Eng. A* 743, 558 <https://doi.org/10.1016/j.msea.2018.04.063> (2019).
39. M.G. Jiang, H. Yan, and R.S. Chen, *Mater. Sci. Eng. A* 621, 204 <https://doi.org/10.1016/j.msea.2014.10.075> (2015).
40. G.M. Zheng, B. Tang, Q. Zhou, X.N. Mao, and R. Dang, *Metals*. 10, 121 <https://doi.org/10.3390/met10010121> (2020).
41. L. Balogh, R.B. Figueiredo, T. Ungár, and T.G. Langdon, *Mater. Sci. Eng. A* 528, 533 <https://doi.org/10.1016/j.msea.2010.09.048> (2010).

Publisher's Note Springer Nature remains neutral with regard to jurisdictional claims in published maps and institutional affiliations.

Springer Nature or its licensor (e.g. a society or other partner) holds exclusive rights to this article under a publishing agreement with the author(s) or other rightsholder(s); author self-archiving of the accepted manuscript version of this article is solely governed by the terms of such publishing agreement and applicable law.